



SCMT4
Las Vegas, USA, August 7-11, 2016

Influence of rGO, n-Al₂O₃ and n-SiO₂ Nanomaterials on the Microstructure of OPC Paste Immersed in 0.5 M HNO₃ Solution

Murugan M.^{1a}, and Manu Santhanam^{1b}

¹*Building Technology and Construction Management Division, Department of Civil Engineering, Indian Institute of Technology Madras, Chennai, Tamil Nadu, Pincode 600036, INDIA.*

^{1a}*Email: <murugan88m@gmail.com>, ^{1b}Email: <manusanthanam@gmail.com>.*

ABSTRACT

Low pH exposure of hydrated cement leads to its gradual degradation by the process of leaching, which is the migration of Calcium ions to the external solution. This action increases the pore connectivity of C-S-H gel and changes its equilibrium Ca/Si ratio. The effect of nanomaterials such as reduced graphene oxide (rGO), dry aluminium oxide nanopowder (n-Al₂O₃) and colloidal silicon dioxide nanoparticles (n-SiO₂) on the Calcium leaching of cement paste was investigated in this paper. The limewater cured cement paste mixes incorporating the nanomaterials were immersed in 0.5 M HNO₃ solution for 56 days. The leached samples were characterized using FTIR, OM, SEM and X-ray CT.

INTRODUCTION

Calcium leaching is several orders higher in acids in comparison to neutral/pure water (Adenot and Buil 1992; Bertron et al. 2005; Gutberlet et al. 2015). The mechanical and durability properties of cement based materials are affected due to acidic/neutral environments. Ionic diffusion takes place between the matrix and the external solution due to difference in concentration of Ca²⁺ and OH⁻ ions within them. Subsequently, the migration of H⁺ ions from the acid into the skeleton of hydrated cement decreases its alkalinity (Pavlík 1994; Beddoe and Dorner 2005; Jacques et al. 2010).

When pH falls below 12.5 Portlandite is the first compound to destabilize followed by decalcification of C-S-H and other hydrates (Pavlík 1994; Hidalgo et al. 2007). The degradation kinetics is rapid and severe until the acidic solution retains its aggressiveness. During such course of action, insoluble salts are formed due to reaction between the Ca²⁺ ions (soluble) and the external solution. However, the insoluble elements retained in the cementitious matrix form a corrosive layer across its cross section. The corroded layer is composed of hydrous form of silicon dioxide, iron and aluminium hydroxides (Pavlík 1994; Moranville et al. 2004; Zivica et al. 2012).

In recent literature, the reduction in Calcium leaching by the addition of silica nanoparticles in Portland cement has garnered attention towards determining the influence of popularly reviewed nanomaterials such as carbon nanotube, graphene and nano alumina on this durability issue (Gaitero et al. 2006; Gaitero et al. 2008; Gaitero et al. 2009; Mondal et al. 2010; Kong et al. 2012; Singh et al. 2013). Owing to the higher surface to volume ratio of the nanomaterials that can act as nucleation sites for cement hydration products, cement hydration is accelerated. Dispersibility of nanomaterials in cement is a major concern in achieving the desired properties which can be overcome by functionalizing them with polymeric groups

(Konsta-Gdoutos et al. 2010; Collins et al. 2012). There were reports in the literature that the addition of graphene oxide nanosheets in cement paste was found to decrease the fraction of unhydrated cement. Such nanosheets act as nucleation sites for the increased growth and production of cement hydrates (Lv et al. 2014; Gong 2015).

This study determines the effect of nanomaterials such as reduced graphene oxide (rGO), dry aluminium oxide nanopowder (n-Al₂O₃) and colloidal silicon dioxide nanoparticles (n-SiO₂) on the microstructure of cement paste which is immersed in 0.5 M HNO₃ solution for 10, 28 and 56 days. The paper also provides the outcome obtained from a combination of microanalytical techniques such as X-ray computed tomography, optical and scanning electron microscopy.

EXPERIMENTAL PROGRAM

Materials

53 Grade ordinary Portland cement (OPC) conforming to IS 12269-1987 and deionized water was used for paste preparation. Table 1 shows the chemical composition of the cement.

Table 1. Chemical composition of 53 grade ordinary Portland cement used in this study

Name of the Compound	CaO	SiO ₂	Al ₂ O ₃	Fe ₂ O ₃	SO ₃	MgO	Cl
Percentage by weight	62.16	20.95	5.14	3.06	3.08	1.33	0.009

Reduced graphene oxide (rGO) was extracted from natural graphite using Modified Hummers method. The synthesizing methods of rGO dispersion in water were followed similar to the procedure adopted in Sen Gupta et al. (2011). In this literature, the resultant rGO sheets were determined to have size fraction in between 5 nm to 1500 nm. The remaining nanomaterials such as n-Al₂O₃ and n-SiO₂ having mean particle size of 50 nm and 12 nm respectively were obtained from Sigma Aldrich, India. Figure 1 shows the SEM/EDS data of the different nanomaterials.

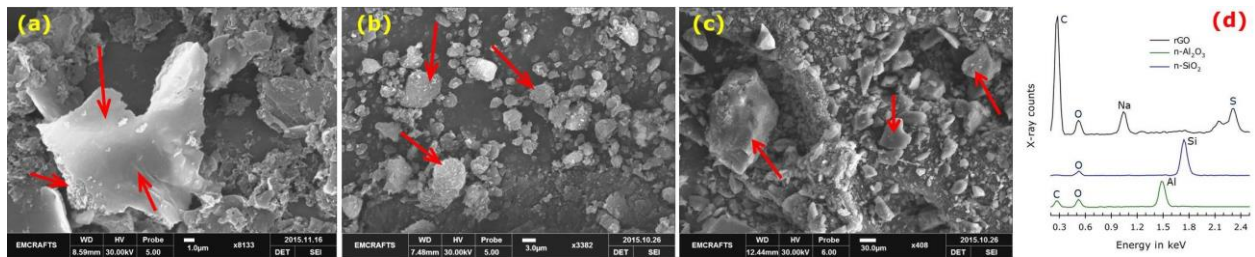


Figure 1. Micrograph illustrating the (a) wrinkled reduced graphene oxide nanoplatelets (b) highly agglomerated Al₂O₃ nanopowder (c) bundled SiO₂ nanoparticles having smooth texture and (d) EDS data showing the presence of impurities (Na and S) in synthesized rGO sheets and the other two nanomaterials (Al₂O₃ and SiO₂) used in this study

Sample preparation and testing methods

Four different cement paste mixes were prepared for this study. One mix was kept as reference whereas the remaining three mixes were incorporated with different nanomaterials such as rGO, n-Al₂O₃ and n-SiO₂ at concentrations of 0.02%, 0.20% and 4.0% by weight of cement respectively. All the mixes were prepared with a w/c ratio of 0.32 and polycarboxylate ether (PCE) based superplasticizer of 0.05% by weight of cement was used for better dispersion of nanomaterials in cement paste at the time of mixing. Ultrasonication of nanomaterials was conducted for 30 minutes using a probe sonicator. Vibration table

was used for the compaction of all pastes. The effect of nanomaterials on the mechanical properties of OPC paste was determined by conducting compressive and flexural strength tests. The paste mixes were demolded after 24 hours and then limewater cured for 7 and 28 days before testing for the strength. The paste specimens of size 25 mm x 25 mm x 25 mm and 20 mm x 20 mm x 160 mm were prepared for determining compressive and flexural strength, which were tested under a loading rate of 143 N/sec and 50 N/sec respectively in a Controls C9842 testing machine. Before immersion in acidic solution, the 28 days limewater cured specimens were designated as t+0.

Accelerated Calcium leaching test

For the leaching test, cement paste prisms of size 10 mm x 10 mm x 50 mm were prepared using acrylic moulds. To study the chemical and phase changes due to Calcium leaching, the prism specimens were immersed in 0.5 M nitric acid (HNO₃) solution for the degradation period of 56 days. The pH value of external solution was measured using a Eutech pH meter. The original pH value was observed as zero which is expressed as ‘highly acidic’ in nature. To maintain the same accelerating effect throughout the test, the external solution was replenished periodically whenever the pH value was increased to 4 or more. This increment occurs due to the migration of alkalis and OH⁻ ions from the hydrated cement to the external solution (Pavlík 1994). To avoid carbonation effect, the specimens were stored inside a glove box chamber which was entirely purged with N₂ (inert) gas. The specimens under test were collected at frequent intervals such as 10, 28 and 56 days and named as t+10, t+28 and t+56 respectively. The alterations in microstructure of pastes due to the effect of leaching were characterized using Emcrafts high resolution scanning electron microscopy (SEM/EDS) and Perkin Elmer Fourier Transform infrared spectroscopy (FTIR). GE Motors X-ray computed tomography (CT) and Olympus optical microscopy (OM) were utilized to obtain the macroscopic images of the leached sample.

RESULTS AND DISCUSSION

Compressive and flexural strength

Figure 2a-b presents the compressive and flexural strength test results of the different pastes cured in saturated lime water solution for 7 and 28 days. The results show that the addition of nanomaterials in OPC paste increased the strengths to a significant extent than the control paste after 7 and 28 days. The refinement of pores/voids in paste was the major reason behind increased mechanical properties. The incorporation of rGO in OPC paste at small concentrations (0.02%) was found efficient in strength enhancement when compared to other nanocomposites (n-Al₂O₃ and n-SiO₂). The water dispersibility of rGO nanosheets synthesized using chemical oxidation method is relatively higher in comparison to other nanomaterials (Li et al. 2008). Such kind of better dispersion ability in polar solvents and 2-Dimensional structure of rGO sheets were the key reasons for its good performance when compared to n-Al₂O₃ and n-SiO₂ pastes.

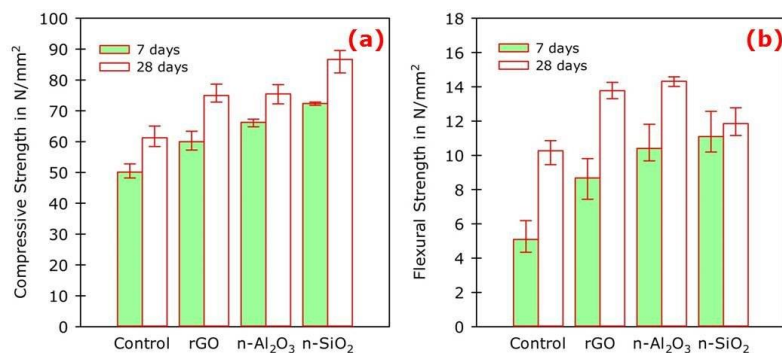


Figure 2. (a) Compressive and (b) flexural strength test results of the different pastes cured for 7 and 28 days

Defect examination using photographs, tomography and microscopy images

Three zones with different colour are formed in hydrated cement due to its immersion in nitric acid solution (Pavlík 1994; Pavlík 1994; Pavlík 1996; Chatveera and Lertwattanaruk 2014). The outermost and the intermediate layer of leached sample are named as ‘white zone’ and ‘brown zone’, which are highly corroded. Pavlik et al. 1994 have reported that the white zone is highly porous, soft and has visible cracks all over its surface. It is predominantly composed of precipitates of SiO_2 and other minor oxides which are insoluble. The reddish brown colour of the intermediate layer is primarily due to the presence of ferric hydroxide and other iron precipitates. The innermost zone of corrosion present in the leached sample is named as ‘grey zone’, which is the sound material. The undamaged part is still occupied with Calcium based hydrated phases. The photograph as shown in Figure 3a indicates the different zones that were formed inside the leached sample after its immersion in 0.5 M HNO_3 solution for 28 days. Figure 3b illustrating the photograph of plain and leached sample collected after 28 and 56 days of degradation. With the help of such photographs, the disappearance of grey zone and the depletion of brown zone with respect to time were clearly observed.

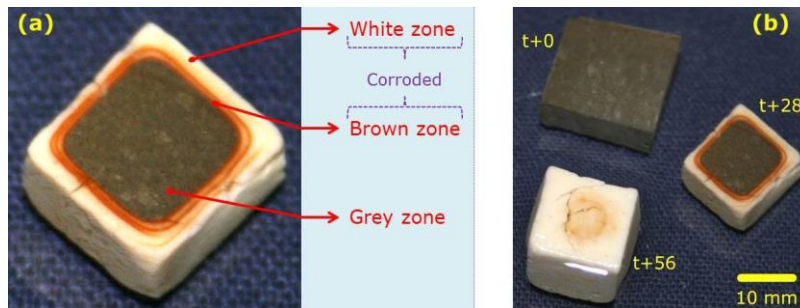


Figure 3. Photographs illustrating (a) the formation of different zones in the leached sample and (b) the plain and the leached sample at different ages

Figure 4a-c shows the pseudo coloured different CT slices of the leached sample (t+28). As stated earlier, the white zone of leached sample crumbles easily due to the formation of wider cracks on its surface as shown in figure 4a. The remaining CT images from figure 4b-c represent the 2D and 3D imaging of different zones formed inside the leached sample.

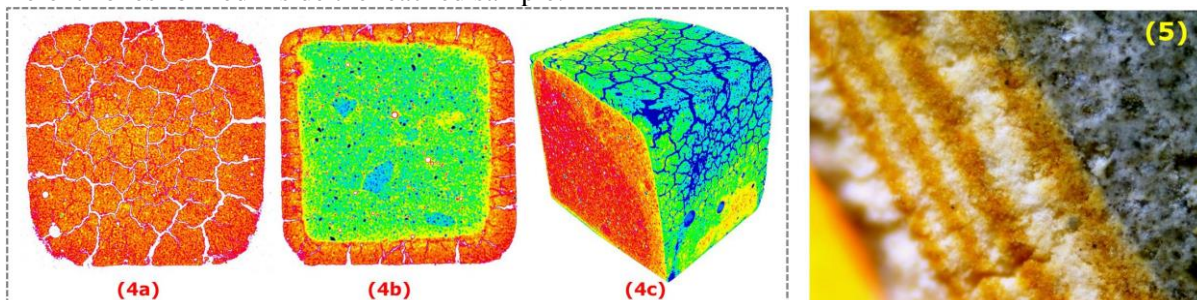


Figure 4. Pseudo coloured CT images of control paste (t+28) illustrating (a) the presence of visible cracks on the white zone, (b) the formation of different zones as well indicating the presence of pores and unhydrated cement and (c) the 3D imaging of leached sample; figure 5. OM image showing the presence of brown rings at equidistant intervals within the corroded region of control paste (t+28)

The presence of pores/voids and unhydrated cement were also visualised in those images. Magnified image of brown zone presented in figure 5 were obtained with optical microscopy. The image suggests

more than three brown rings were formed in the leached sample due to its immersion in 0.5 M HNO₃ solution for 28 days.

IR spectra

Figure 6a-d presents the mid infrared spectra of the different pastes collected at three different intervals such as t+0, t+10 and t+28 respectively.

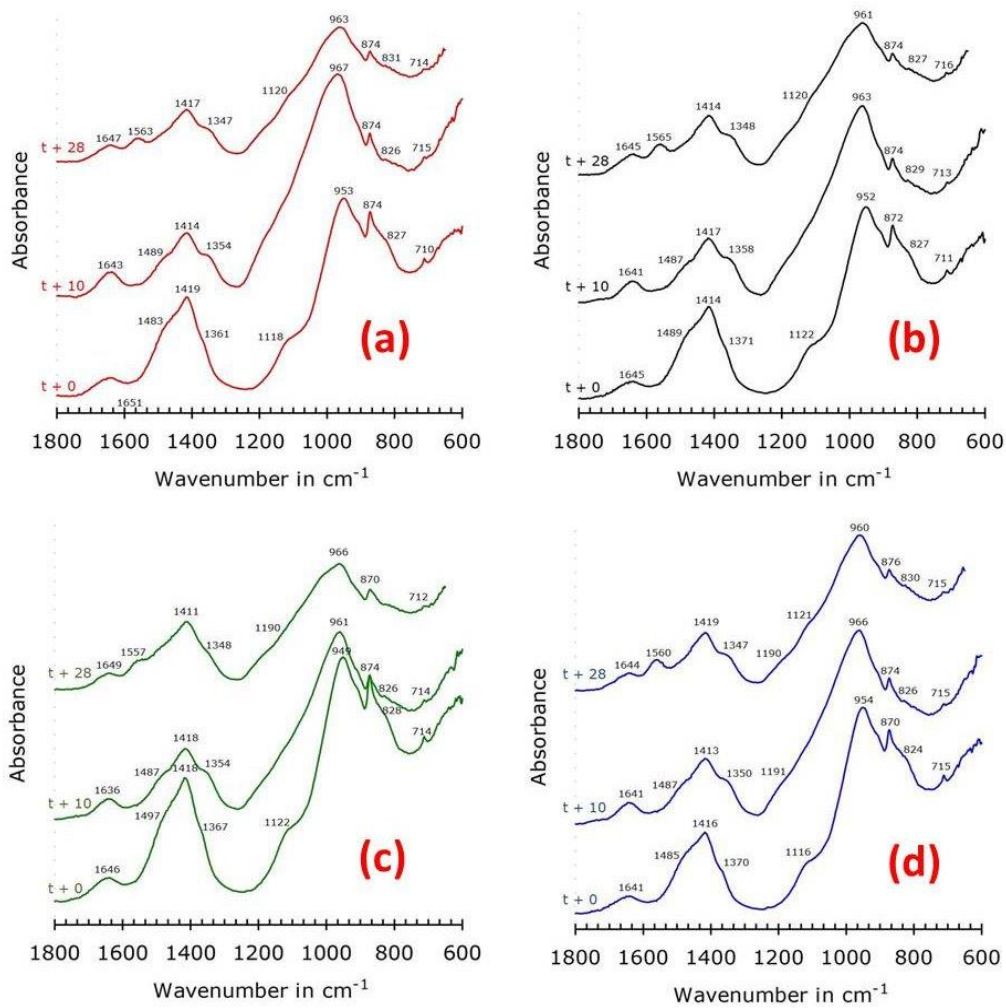


Figure 6. Mid IR spectra of (a) Control (b) rGO (c) n-Al₂O₃ and (d) n-SiO₂ pastes at different intervals like t+0, t+10 and t+28

While analysing the absorption bands, the peak attributed to O-H bend ~ 1647 cm⁻¹ representing the presence of calcium hydroxide were found to diminish at increasing period of degradation. This suggests the disappearance of Portlandite (C-H) from the hydrated cement due to its continuous exposure to acids. However, the peaks attributed to C-O stretch ~ 1414 cm⁻¹ and C-O bend ~ 874 cm⁻¹ vibration representing the presence of CO₃²⁻ shows the increased formation of carbonate minerals in the Calcium leached sample. The wavenumber 963 cm⁻¹ (SiO₄) from the IR spectra specifies the presence of silicates in the leached sample. Finally, the peak attributed to N-O stretch ~ 1563 cm⁻¹ represents the availability of nitro compounds in the leached sample (t+28) which indicates the formation of Calcium nitrate due to its immersion in HNO₃ solution.

SEM images

The SEM analyses were performed on the fractured surface of leached sample to determine the alterations in its microstructure. Figure 7 illustrates the micrograph of the control paste (t+28).

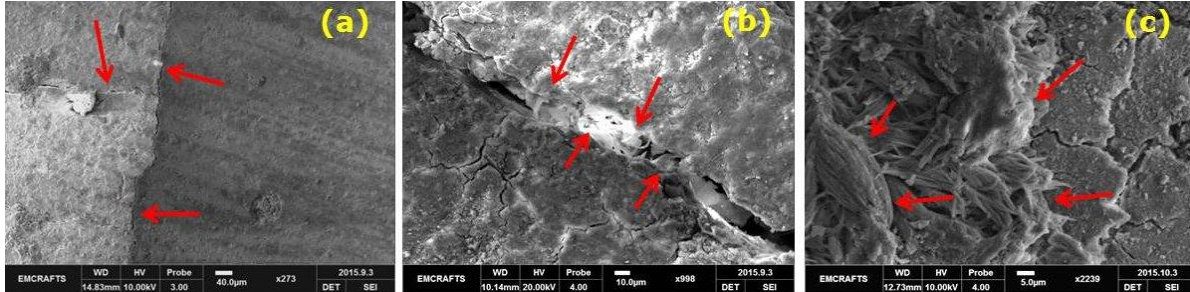


Figure 7. Micrograph of the control paste (t+28) (a) Presence of visible cracks in the leached sample (b) Formation of leaf like compounds inside the crack (c) Deposits of a thick layer of carbonate based minerals with reticulated structure seen in the leached sample

In the leached sample, visible cracks were formed because of C-S-H decalcification and dissolution of other hydrates. Along its cross sectional area, a longitudinal surface crack was found in between the corroded regions and the sound material which is clearly seen in figure 7a. Additionally, multiple cracks were observed in the corroded regions in perpendicular to the major crack. Further leaching of Calcium ions within such crack tends to form leaf like compounds (figure 7b). In figure 7c, the deposition of a thick layer of carbonate based minerals having reticulated (net like intergrowth) structure was identified over the corroded regions of the leached sample. figure 8 illustrates the micrograph of the rGO paste (t+56).

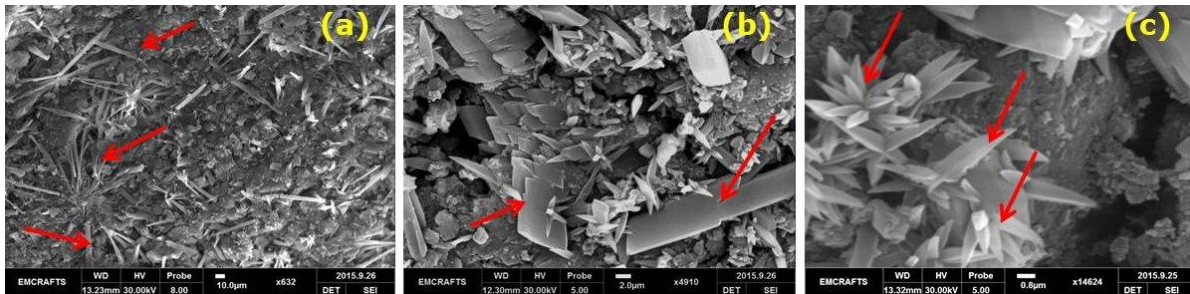


Figure 8. Micrograph illustrating the formation of gypsum based minerals with (a) thin-radiated needle like (b) flat-elongated prismatic and (c) spiky-radiated pyramidal structure present in the brown zone of rGO paste (t+56)

In the brown zone of leached sample, three different crystals with thin-radiated needle like (8a), flat-elongated prismatic (8b) and spiky-radiated pyramidal structure (8c) were formed. The rGO sheets with high surface area act as nucleation sites for the growth and production of cement hydrates (Lv et al. 2014). Figure 1d illustrates the self-synthesized rGO sheets consist of sulfate and sodium residues. The interaction between the Calcium leachate and the sulfate in rGO sheets may lead to the formation of gypsum based minerals with distinct crystalline structure. Figure 9a clearly shows the presence of bundled aluminium oxide nanoparticles in the brown zone of n-Al₂O₃ paste (t+28). In this image, empty pores/voids were present after the removal of such crystalline nanoparticles. The formation of thin-radiated plate like crystals which is densely packed was observed in the brown zone of leached sample as shown in figure 9b. The carbonate based minerals are found to have similar crystalline structure. At the

interface of grey and brown zone presented in figure 9c, spherical shaped crystals with cavity in them were observed.

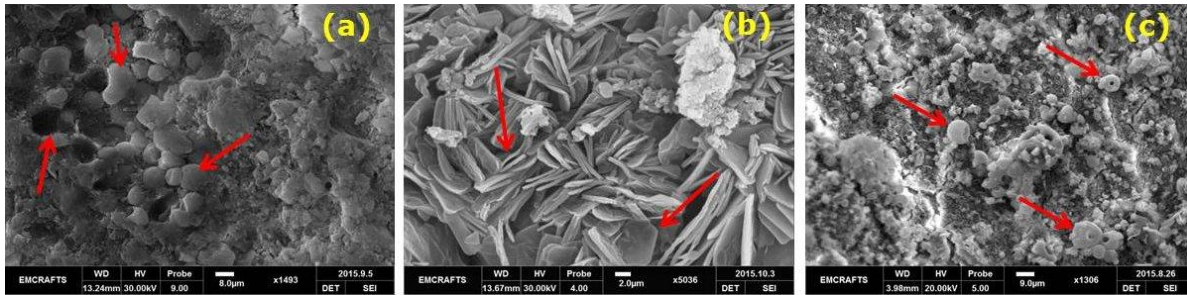


Figure 9. Micrograph showing the brown zone of the n-Al₂O₃ paste (t+28) occupied with (a) agglomerated Al₂O₃ nanoparticles (b) thin-radiated plate like and (c) spherical shaped crystals having cavities

The micrograph of the n-SiO₂ paste (t+28) is shown in figure 10. The brown zone of leached sample as shown in figure 10a was entirely distributed with SiO₂ nanoparticles. figure 10b illustrates the poorly dispersed SiO₂ nanoparticles which are found unreacted with the nearby cement hydrates. The zone was also occupied with the formation of non-uniform, radiated leaf like compounds (figure 10c) which are calcium silicate based minerals.

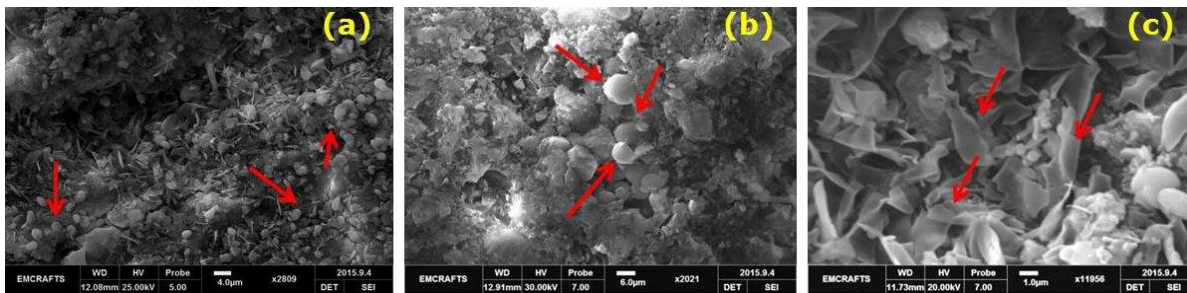


Figure 10. Micrograph illustrating the brown zone of the n-SiO₂ paste (t+28) (a) entirely dispersed with SiO₂ nanoparticles (b) agglomerated nano SiO₂ which are unreacted with the cement hydrates (c) the formation of poorly oriented, leaf like compounds

CONCLUSION

The influence of nanomaterials such as rGO, n-Al₂O₃ and n-SiO₂ on the microstructure of OPC paste due to its immersion in 0.5 M HNO₃ solution, investigated with the help of characterization studies such as SEM/EDS, FTIR, OM and X-ray CT, was reported in this paper. The key findings from this study are listed as follows:

- The nanomaterials addition (rGO, n-Al₂O₃ and n-SiO₂) in OPC paste reduces the amount of pores/voids. This effect increased the compressive and flexural strength of the nanocomposite modified pastes to a significant extent when compared to control paste.
- The macroscopic changes such as presence of visible cracks, pores/voids, unhydrated cement and zone thickness of the leached sample were completely visualised using photographs and tomography images. OM images suggest more than three brown rings were regularly formed on the different pastes due to its immersion in 0.5 M HNO₃ solution for 28 days.
- The formation of nitro compounds in the leached sample was identified using IR spectra. Additionally, the presence of new compounds due to calcium leaching was determined using SEM/EDS. The EDS

data suggest heavy carbonation was followed in all pastes after decalcification of C-S-H and other hydrates. In control paste, calcite compounds with reticulated structure were found occupying the interfacial surface of grey and brown zone of its leached sample (t+28). The presence of calcium carbonate and calcium silicate crystals with plate like structure were identified in leached samples (t+28) of n-Al₂O₃ and n-SiO₂ paste. In rGO paste (t+56), the presence of gypsum based minerals with distinct crystalline structures were found in the brown zone of its leached sample.

REFERENCES

- Adenot, F., and Buil, M. (1992). "Modelling of the corrosion of the cement paste by deionized water." *Cement and Concrete Research*, 22(2–3), 489-496.
- Bertron, A., Duchesne, J., and Escadeillas, G. (2005). "Accelerated tests of hardened cement pastes alteration by organic acids: analysis of the pH effect." *Cement and Concrete Research*, 35(1), 155-166.
- Gutberlet, T., Hilbig, H., and Beddoe, R. E. (2015). "Acid attack on hydrated cement — Effect of mineral acids on the degradation process." *Cement and Concrete Research*, 74, 35-43.
- Pavlík, V. (1994). "Corrosion of hardened cement paste by acetic and nitric acids part I: Calculation of corrosion depth." *Cement and Concrete Research*, 24(3), 551-562.
- Beddoe, R. E., and Dorner, H. W. (2005). "Modelling acid attack on concrete: Part I. The essential mechanisms." *Cement and Concrete Research*, 35(12), 2333-2339.
- Jacques, D., Wang, L., Martens, E., and Mallants, D. (2010). "Modelling chemical degradation of concrete during leaching with rain and soil water types." *Cement and Concrete Research*, 40(8), 1306-1313.
- Hidalgo, A., Petit, S., Domingo, C., Alonso, C., and Andrade, C. (2007). "Microstructural characterization of leaching effects in cement pastes due to neutralisation of their alkaline nature: Part I: Portland cement pastes." *Cement and Concrete Research*, 37(1), 63-70.
- Pavlík, V. (1994). "Corrosion of hardened cement paste by acetic and nitric acids part II: Formation and chemical composition of the corrosion products layer." *Cement and Concrete Research*, 24(8), 1495-1508.
- Moranville, M., Kamali, S., and Guillon, E. (2004). "Physicochemical equilibria of cement-based materials in aggressive environments—experiment and modeling." *Cement and Concrete Research*, 34(9), 1569-1578.
- Zivica, V., Palou, M. T., Krizma, M., and Bagel, L. (2012). "Acidic attack of cement based materials under the common action of high, ambient temperature and pressure." *Construction and Building Materials*, 36, 623-629.
- Gaitero, J. J., Sáez de Ibarra, Y., Erkizia, E., and Campillo, I. (2006). "Silica nanoparticle addition to control the calcium-leaching in cement-based materials." *physica status solidi (a)*, 203(6), 1313-1318.
- Gaitero, J. J., Campillo, I., and Guerrero, A. (2008). "Reduction of the calcium leaching rate of cement paste by addition of silica nanoparticles." *Cement and Concrete Research*, 38(8–9), 1112-1118.
- Gaitero, J. J., Zhu, W., and Campillo, I. (2009). "Multi-scale Study of Calcium Leaching in Cement Pastes with Silica Nanoparticles." *Nanotechnology in Construction 3*, Z. Bittnar, P. M. Bartos, J. Němeček, V. Šmilauer, and J. Zeman, eds., Springer Berlin Heidelberg, 193-198.
- Mondal, P., Shah, S., Marks, L., and Gaitero, J. (2010). "Comparative study of the effects of microsilica and nanosilica in concrete." *Transportation research record: journal of the transportation research board*(2141), 6-9.

- Kong, D., Du, X., Wei, S., Zhang, H., Yang, Y., and Shah, S. P. (2012). "Influence of nano-silica agglomeration on microstructure and properties of the hardened cement-based materials." *Construction and Building Materials*, 37, 707-715.
- Singh, L. P., Karade, S. R., Bhattacharyya, S. K., Yousuf, M. M., and Ahalawat, S. (2013). "Beneficial role of nanosilica in cement based materials – A review." *Construction and Building Materials*, 47, 1069-1077.
- Konsta-Gdoutos, M. S., Metaxa, Z. S., and Shah, S. P. (2010). "Highly dispersed carbon nanotube reinforced cement based materials." *Cement and Concrete Research*, 40(7), 1052-1059.
- Collins, F., Lambert, J., and Duan, W. H. (2012). "The influences of admixtures on the dispersion, workability, and strength of carbon nanotube–OPC paste mixtures." *Cement and Concrete Composites*, 34(2), 201-207.
- Lv, S., Liu, J., Sun, T., Ma, Y., and Zhou, Q. (2014). "Effect of GO nanosheets on shapes of cement hydration crystals and their formation process." *Construction and Building Materials*, 64, 231-239.
- Gong, K., Pan, Z., Korayem, A.H., Qiu, L., Li, D., Collins, F., Wang, C.M., and Duan, W.H. (2015). "Reinforcing Effects of Graphene Oxide on Portland Cement Paste." *Journal of Materials in Civil Engineering*, 27(2), A4014010.
- Sen Gupta, S., Manoj Siva, V., Krishnan, S., Sreeprasad, T. S., Singh, P. K., Pradeep, T., and Das, S. K. (2011). "Thermal conductivity enhancement of nanofluids containing graphene nanosheets." *Journal of Applied Physics*, 110(8), 084302.
- Li, D., Muller, M. B., Gilje, S., Kaner, R. B., and Wallace, G. G. (2008). "Processable aqueous dispersions of graphene nanosheets." *Nat Nano*, 3(2), 101-105.
- Pavlík, V. (1996). "Corrosion of hardened cement paste by acetic and nitric acids Part III: Influence of water/cement ratio." *Cement and Concrete Research*, 26(3), 475-490.
- Chatveera, B., and Lertwattanaruk, P. (2014). "Evaluation of nitric and acetic acid resistance of cement mortars containing high-volume black rice husk ash." *Journal of Environmental Management*, 133, 365-373.
- Lv, S., Ting, S., Liu, J., and Zhou, Q. (2014). "Use of graphene oxide nanosheets to regulate the microstructure of hardened cement paste to increase its strength and toughness." *CrystEngComm*, 16(36), 8508-8516.